Polarimetric Studies of a Fast Coronal Mass Ejection

Marilena Mierla[1,2] · Bernd Inhester[3] · Andrei N. Zhukov[1,4] ·
Sergei V. Shestov[1] · Alessandro Bemporad[5] · Philippe Lamy[6] · Serge Koutchmy[7]

Abstract

In this work we performed a polarimetric study of a fast and wide coronal mass ejection (CME) observed on 12 July 2012 by the COR1 and COR2 instruments onboard the *Solar TErrestrial RElations Observatory* (STEREO) mission. The CME source region was an X1.4 flare located at approximately S15W01 on the solar disk, as observed from the Earth's perspective. The position of the CME as derived from the 3D Graduated Cylindrical Shell (GCS) reconstruction method was at around S18W00 at 2.5 solar radii and S07W00 at 5.7 solar radii, meaning that the CME was deflected towards the Equator while propagating outward in the corona. The projected speed of the leading edge of the CME also evolved from around $200 \, \mathrm{km \, s^{-1}}$ in the lower corona to around $1000 \, \mathrm{km \, s^{-1}}$ in the COR2 field of view. The degree of polarisation of the CME is around 65% but it can go as high as 80% in some CME regions. The CME showed deviation of the polarisation angle from the tangential in the range of $10 - 15°$ (or more). Our analysis showed that this is mostly due to the fact that the sequence of three polarised images from where the polarised parameters are derived is not taken simultaneously, but at a difference of a few seconds in time. In this interval of time, the CME moves by at least two pixels in the FOV of the instruments and this displacement results in uncertainties in the polarisation parameters (degree of polarisation, polarisation angle, etc.). We propose some steps forward to improve the derivation of the polarisation. This study is important for analysing the future data from instruments with polarisation capabilities.

Keywords Corona, K · Corona, active · Polarisation, optical · Coronal mass ejections

1. Introduction

The white-light emission of the solar K-corona originates in Thomson scattering of photospheric light by free electrons in the corona. Detailed descriptions of the Thomson-scattering theory can be found in various articles (see, e.g., Minnaert, 1930; Baumbach, 1938; van de Hulst, 1950; Shklovskii, 1965; Billings, 1966; Inhester, 2015).

It is known that the degree of polarisation of Thomson-scattered light by coronal electrons is a sensitive function of the scattering angle between the incident-light direction and the direction towards the observer (Billings, 1966). This effect allows us to estimate an effective distance of the coronal-scattering volume off the plane of the sky (POS), and it has been employed to obtain 3D positions of coronal mass ejections (CMEs) from coronagraph

---

images obtained with different polariser orientations (see, e.g., Moran and Davila, 2004; Dere, Wang, and Howard, 2005; Vourlidas and Howard, 2006; Mierla et al., 2009).

In a recent study, Floyd and Lamy (2019), taking advantage of the much improved determination of the polarisation of the corona (see, e.g., Lamy et al., 2014) from the LASCO-C2 images (Brueckner et al., 1995), applied the polarised-ratio technique to a set of 15 CMEs observed in the time interval from 1998 to 2014. The authors showed that despite the unfavourable conditions affecting the LASCO-C2 polarisation measurements, the polarimetric reconstruction works quite well and is able to produce meaningful 3D CME morphology and direction of propagation. Even in the case of the very fast CME of 18 July 2002 (speed around 2000 km s^{-1}), its localisation could be obtained for the bulk of it (Floyd and Lamy, 2019).

As the observed polarised brightness is much less sensitive to stray light, it has been also widely used to estimate the electron density of the average corona and of the total mass of CMEs (see, e.g., Quémerais and Lamy, 2002; Feng et al., 2015; Decraemer, Zhukov, and Van Doorsselaere, 2019). As the estimation of the CME mass and propagation direction has important implications for space-weather forecasts, it is important to have accurate measurements of the polarisation parameters.

The accurate measurements of the polarisation parameters can be checked by the tangential orientation of the polarisation direction. There are limits to this check, both experimental (mirrors may rotate the polarisation (Floyd and Lamy, 2019), atmospheric effects for ground-based measurements (see Koutchmy et al., 1999), limited precision, etc.), and theoretical (non-random orientation of dust, relativistic electrons (Molodensky, 1973; Kishonkov and Molodenskii, 1975), and magnetically sensitive resonant-line scattering (see, e.g. Mierla et al., 2011; Qu et al., 2013; Heinzel et al., 2020). In this article we present the observation of a systematic deviation of the polarisation angle. This deviation occurs near the propagation front of a fast CME. This led us to the conclusion that we have to account for yet another effect that may lead to rotated polarisation angles. This effect has so far not been considered in the literature. We discuss this effect quantitatively and compare it with possible alternative reasons in the discussion section. The article is structured as follows: In Section 2 we introduce the data, and in Sections 3 and 4 we describe how they are processed and analysed. Discussions and conclusions are presented in Sections 5 and 6, respectively.

2. Observations

In this work, we use COR1 and COR2 images taken on 12 July 2012. COR1 is the coronagraph with the innermost field of view of the *Sun Earth Connection Coronal and Heliospheric Investigation* (SECCHI) instrument suite (Howard et al., 2008) onboard the twin *Solar TErrestrial RElations Observatory* spacecraft (STEREO: see Kaiser et al., 2008). Each of the STEREO/COR1 telescopes has a field of view from 1.4 to 4 solar radii [$R_\odot$] and observes in a white-light waveband 22.5 nm wide centred at the Hα line at 656 nm (Thompson and Reginald, 2008).

Like the COR1, the SECCHI outer field-of-view coronagraph, COR2, observes the coronal signal in visible light from 2 to 15 $R_\odot$, with a passband from 650 to 750 nm. Both COR1 and COR2 coronagraphs take polarised images at three different polarisation angles at 0°, 120°, and 240°.

The COR1 images have dimensions of 512×512 pixels and a pixel size of 15″. The exposure time is one second and the image cadence is five minutes. Each set of three polarised images (I_0, I_{120}, and I_{240}) is taken in approximately 18 seconds (COR1-A) and 24 seconds

(COR1-B), with 9 seconds between the frames in the case of COR1-A data, and 12 seconds between the frames for COR1-B.

The COR2 images have dimensions of 2048×2048 pixels and a pixel size of $15''$. The exposure time is six seconds and the image cadence is one hour. Each set of three polarised images (I_0, I_{120}, and I_{240}) is taken in approximately 60 seconds with 30 seconds between the frames.

On 12 July 2012, a fast and wide CME (associated with an X1.4 flare) was observed at the east limb on COR-A images, at the west limb in COR-B images, and coming from the central disk in LASCO images. The approximate location of the CME source region (the X1.4 flare) was S15W01 as observed from the Earth's perspective (see, e.g., cdaw.gsfc. nasa.gov/CME_list/halo/halo.html and solarmonitor.org/index.php?date=20120712&region= 11520).

The CME was observed for the first time by COR1 at around 16:00 UT, by COR2 at around 16:40 UT, and by LASCO-C2 at around 16:50 UT. COR1 and COR2 coronagraphs observed a structured, three-part CME consisting of a bright circular leading edge, followed by a dark cavity and a bright compact core (see, e.g., Illing and Hundhausen, 1986), while LASCO-C2 and -C3 coronagraphs observed a full-halo CME with apparent angular width of 360°. A diffuse shock (see, e.g., Vourlidas et al., 2003) was also observed ahead of the leading edge.

3. Data Processing

Data processing consists of three steps:

  i) Pre-process the data using the IDL SolarSoft secchi_prep.pro routine.
 ii) Extract the K-corona signal by subtraction of the base-difference image.
iii) Extract the polarised parameters – polarised brightness, total brightness, degree of polarisation, and the deviation angle from the tangential – from three K-corona images with different polarisations I_0, I_{120}, and I_{240}.

3.1. Data Pre-Processing

We run secchi_prep on each polarised COR1 and COR2 image. By default, secchi_prep applies the following calibration to COR images: division by exposure duration; correction for onboard image processing; subtraction of the CCD bias; multiplication by the calibration factor to convert the image values from digital number (DN) to mean solar brightness (MSB); vignetting and flat-field correction; and optical distortion correction (COR2 only).

The COR1 and COR2 images were brought to the same dimensions: 1024×1024 pixels with the pixel size of $7.5''$ for COR1 and $29.4''$ for COR2.

We divided each image by the calibration factor 6.780×10^{-11} for COR1 and 1.350×10^{-12} for COR2 to have units of DN s^{-1}. We preferred DN s^{-1} as it offers a more straightforward way to display the data. The choice of the units does not influence our results.

3.2. Extracting K-Corona Signal

In general, one raw white-light coronagraph image contains signal from the solar corona (K-corona: electron or continuum corona; F-corona: Fraunhofer or dust corona; E-corona:
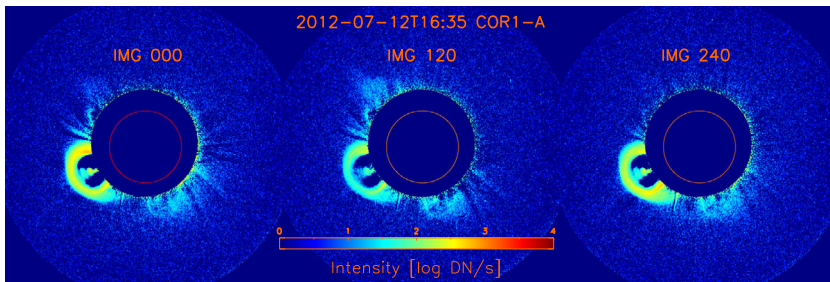
Figure 1 COR1 images taken on 12 July 2012, with orientation of the polariser of 0° taken at 16:35:00 UT (*left panel*), 120° at 16:35:09 UT (*middle panel*), and 240° at 16:35:18 UT (*right panel*). Images are displayed on a logarithmic scale. Base-difference images were used. The radius of the occulter is 1.47 R$_\odot$ and the circle inside the occulter outlines the solar disk.

emission lines like Hα, Fe X, Fe XIV, Ca XV, He I D3 line, etc.), from the cosmic rays, planets, comets, stars, as well as from the instrument-related contribution: bias, dark current, stray light, etc. Some of this signal is polarised, and some is unpolarised.

The K-corona signal is due to the scattering of the sunlight (photospheric light) by the free electrons of the corona, also known as the Thomson-scattered light. The F-corona is the scattering of the light on the dust particles around the Sun (contains Fraunhofer absorption lines). The E-corona is formed from the emission of highly ionised atoms of the solar corona. One more component, the thermal (T-corona) is produced by thermal emission of dust particles heated by the Sun (Shopov et al., 2008).

The K-corona contains features such as streamers, CMEs, outflows, inflows, etc. In the ideal case we would like to eliminate all the unwanted contributions and keep the signal only from the K-corona, or in our case only from the CME Thomson-scattered light. In order to eliminate the unwanted signal, one can employ different procedures: i) subtraction of the monthly minimum background from a raw white-light coronagraph image; ii) subtraction of a pre-event image from a raw white-light coronagraph image (the so-called base-difference image technique); iii) subtraction of an hourly minimum background from a raw white-light coronagraph image.

These procedures are described in detail in Appendix A.

For this study we used base-difference images by subtracting the frame before the CME was observed, at 15:50 UT in COR1 and at 16:09 UT in the COR2 field of view (FOV). Three different pre-event images are used, one each for the three polarisers. Henceforth, if not stated otherwise we will always be using base-difference images.

The influence of different backgrounds on our results is discussed in Appendix B.

Figure 1 shows an example of one set of three polarised COR1-A images taken on 12 July 2012, 16:35 UT.

3.3. Extraction of the Polarisation Parameters

From COR1 and COR2 polarised images processed as explained above, we derived polarised quantities: total brightness (B – Equation 1), polarised brightness (pB – Equation 2), the degree of polarisation (p – Equation 3), and the polarisation-angle orientation (α – Equation 4) of the K-corona signal. The deviation angle from the tangential [$\Delta\alpha$] is calculated as the difference between the tangent to the solar limb and the polarisation angle. Positive values of the deviation angle correspond to the clockwise rotation and the negative values to

the counter-clockwise rotation.

$$B = \frac{2}{3}\left(I_0 + I_{120} + I_{240}\right) \tag{1}$$

$$pB = \frac{4}{3}\sqrt{(I_0 + I_{120} + I_{240})^2 - 3\left(I_0 I_{120} + I_0 I_{240} + I_{120} I_{240}\right)} \tag{2}$$

$$p = \frac{pB}{B} \tag{3}$$

$$\alpha = \frac{1}{2}\arctan\frac{\sqrt{3}\left(I_{240} - I_{120}\right)}{2I_0 - I_{120} - I_{240}}. \tag{4}$$

These formulae correspond to frequently used ones that utilise Stokes parameters I, Q, and U. Here, we use explicit formulae to simplify the analysis presented in Section 4.2. In Equation 1 and Equation 2 we used the directions of 0°, 120°, and 240° of the polarisers, instead of the usual directions of 0°, 60°, and 120° because these are the angles at which the COR1 polarisers are reported to be oriented, (see, e.g., Thompson and Reginald, 2008). Note that 60° and 240° polariser orientations are identical.

I_0, I_{120}, and I_{240} represent the images recorded by the COR1 instrument at three polarisation angles, from which a pre-event image was subtracted as mentioned in the previous section. In this way, the three polarised images I_0, I_{120}, and I_{240} contain largely only the component of the CME K-corona.

The polarisation angles for COR2 images were corrected with the values provided by the SolarSoft routine cor1_fitpol.pro (Thompson, 2015). This was necessary because the COR2 polarisers do not have a specific alignment.

4. Data Analysis and Interpretation

4.1. CME Polarisation Parameters

In Figure 2 we show the extracted polarisation parameters from COR1-A images taken at 16:35 UT (left column) and at 16:50 UT (right column), as follows: polarised brightness pB (upper panels), total brightness B (middle-upper panels), degree of polarisation p (middle-lower panels), and deviation angle from the tangential (lower panels).

We observe deviations from the tangential greater than 10°, in regions associated with the excess brightness of the CME (see also Figure 3). The degree of polarisation is around 70% in regions associated with the CME signal (see also Figure 3).

We apply the same technique to COR1-B and COR2-A and -B images, to see if the same behaviour is observed in different instruments.

Figure 4 displays the total brightness calculated from COR1-A (upper-left panel), COR1-B (upper-right panel), COR2-A (lower-left panel) and COR2-B (lower-right panel) images. The images are shown on a logarithmic scale. The two COR-B images show a rather consistent structure of the CME, whereas the COR2-A structure is much more complex than the COR1-A one.

Figure 5 shows the degree of polarisation from COR1-A (upper-left panel), COR1-B (upper-right panel), COR2-A (lower-left panel) and COR2-B (lower-right panel).

The degree of polarisation is around 65% but it can go as high as 80% in some CME regions from COR1-A. These high values of the degree of polarisation are more observed in COR2 images.

Figure 2 COR1-A polarisation parameters derived from polarised images on 12 July 2012, 16:35 UT (*left panels*) and 16:50 UT (*right panels*) showing: *pB*-images (*upper panels*), *B*-images (*middle-upper panels*), degree of polarisation (*middle-lower panels*) and deviation from the tangential angle (*lower panels*). *pB* and *B* images are displayed on a logarithmic scale. The parameters are derived from base-difference images. The circle inside the occulter outlines the solar disk.
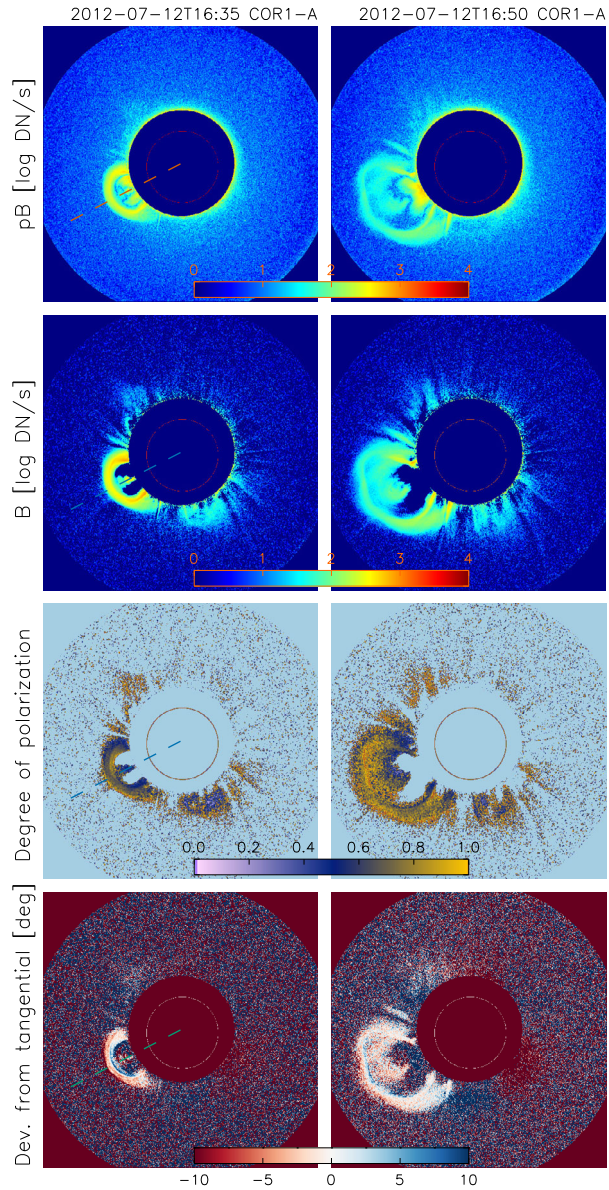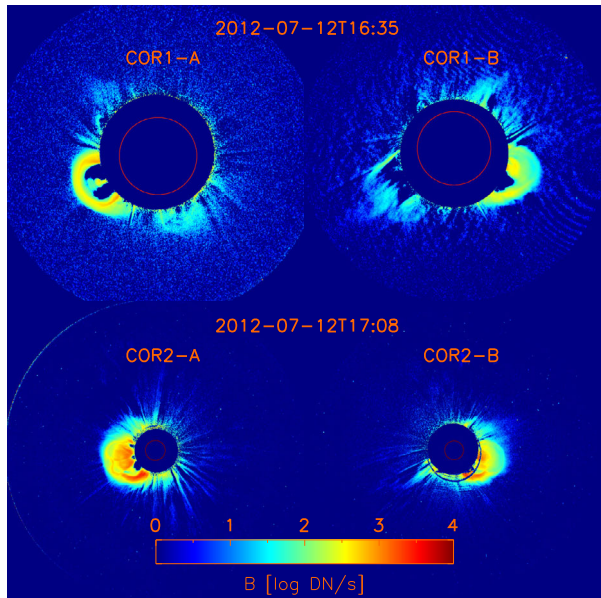

In Figure 6 is shown the deviation angle from the tangential using COR1-A (upper-left panel), COR1-B (upper-right panel), COR2-A (lower-left panel), and COR2-B (lower-right panel) data.

Deviations from the tangential up to $10 - 15°$ are seen in COR1-A images (upper-left panel of Figure 6), in all pixels where a significant CME excess brightness is observed, i.e. in both the front and the core of the CME (see also Figure 2). It is more visible on the front part of the CME (the red and blue areas in the front and back part of the CME frontal structure). The deviations are smaller in COR1-B images. The same deviations are observed
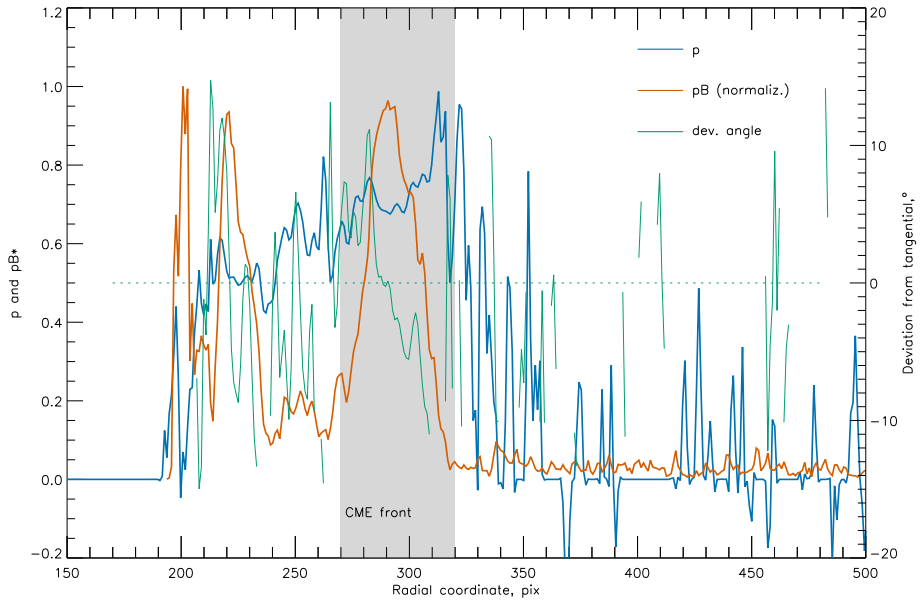
Figure 3 Radial profiles of the polarisation parameters along the dashed line in Figure 2.
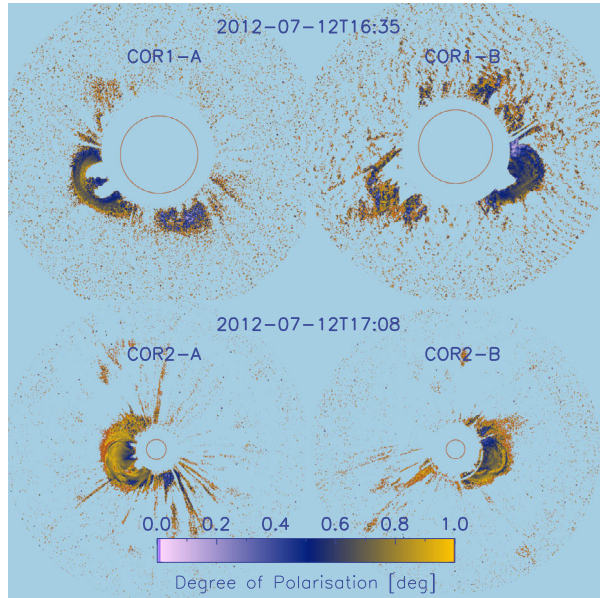

Figure 4 Total brightness from COR1-A (*upper-left panel*), COR1-B (*upper-right panel*), COR2-A (*lower-left panel*), and COR2-B (*lower-right panel*) observations. The images are displayed on a logarithmic scale. Base-difference images were used. The circle inside the occulter outlines the solar disk.

also in monthly minimum and hourly minimum background subtracted images, as discussed in Appendix B. For COR1, a systematic constant deviation of the polarisation angle by $-1°$ was found (Inhester et al., 2021).

For COR2-A data, the deviation from the tangential increases to $30°$ at the front of the CME (blue area in the lower-left panel of Figure 6).

Figure 5 Degree of polarisation from COR1-A (*upper-left panel*), COR1-B (*upper-right panel*), COR2-A (*lower-left panel*), and COR2-B (*lower-right panel*) observations. Base-difference images were used. The circle inside the occulter outlines the solar disk.

Figure 6 Deviation angle from the tangential from COR1-A (*upper-left panel*), COR1-B (*upper-right panel*), COR2-A (*lower-left panel*), and COR2-B (*lower-right panel*) observations. Base-difference images were used. The circle inside the occulter outlines the solar disk.
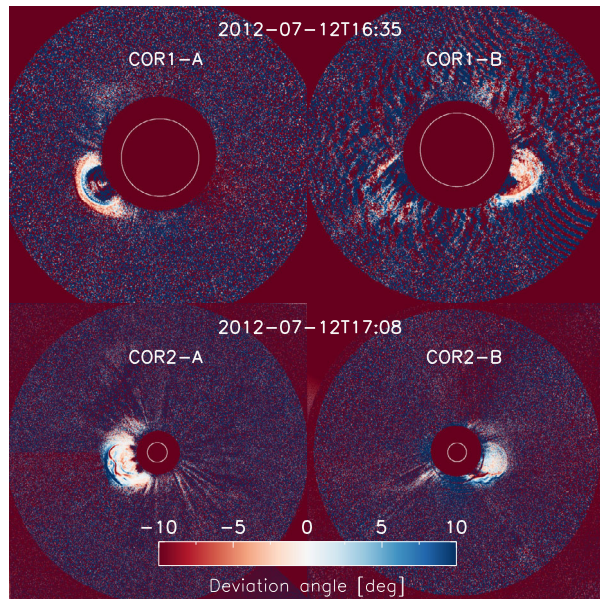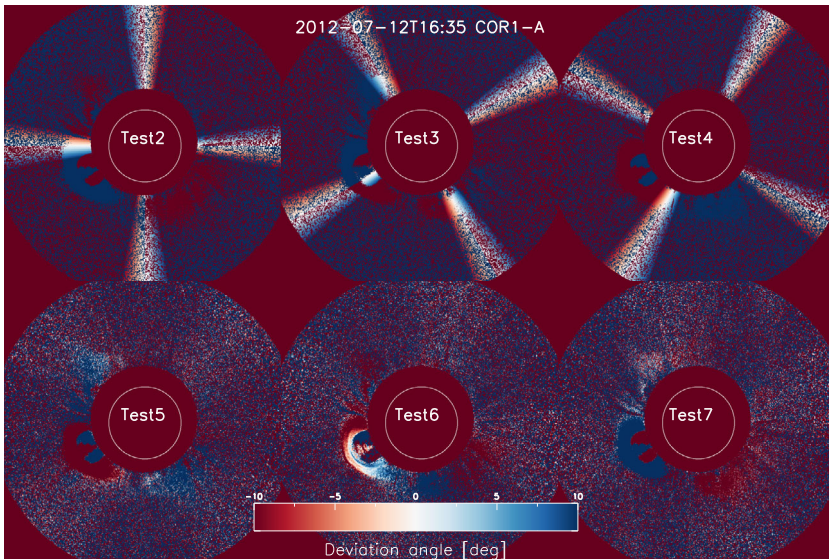
4.2. Tests on Deviation from the Tangential

To further investigate the deviations from the tangential described above, we perform a few tests, as displayed in Figure 7. We used base-difference COR1-A images, at 16:35 UT for these tests.

Figure 7 Deviation angle from the tangential calculated in six different scenarios: *Upper row*, from *left to right*: I_{120} and I_{240} set to zero, I_0 as observed; I_0 and I_{240} set to zero, I_{120} as observed; I_0 and I_{120} set to zero and I_{240} as observed. *Lower row*, from *left to right*: I_0 set to zero and I_{120} and I_{240} as observed; I_{120} set to zero and I_0 and I_{240} as observed; I_{240} set to zero and I_0 and I_{120} as observed. The circle inside the occulter outlines the solar disk.

i) In the first test (upper-left panel in Figure 6), we derive the polarisation angle from the three polarised images (I_0, I_{120}, and I_{240}) recorded by COR1-A at 16:35 UT.

ii) For the second test (left image of the upper row in Figure 7), we kept I_0 as observed and assigned I_{120} and I_{240} a zero value in all pixels.

iii) For the third test (middle image of the upper row in Figure 7), we kept I_{120} as observed and assigned I_0 and I_{240} a zero value in all pixels.

iv) For the fourth test (right image of the upper row in Figure 7), we kept I_{240} as observed and assigned I_0 and I_{120} a zero value in all pixels.

v) For the fifth test (left image of the lower row in Figure 7), we kept I_{120} and I_{240} as observed and assigned I_0 a zero value in all pixels.

vi) For the sixth test (middle image of the lower row in Figure 7), we kept I_0 and I_{240} as observed and assigned I_{120} a zero value in all pixels.

vii) For the seventh test (right image of the lower row in Figure 7), we kept I_0 and I_{120} as observed and assigned I_{240} a zero value in all pixels.

We see that the observed deviation angles are almost entirely due only to the combination of I_0 and I_{240} images, which are taken 18 seconds apart. In this time interval, a CME with a speed of $600\,\mathrm{km\,s^{-1}}$ will move about 10,800 km, i.e. more than two pixels ($= 10,489.8\,\mathrm{km}$) in COR1-A FOV, which may justify the deviations observed. The speed of $600\,\mathrm{km\,s^{-1}}$ was the measured speed of the CME at $2.41\,\mathrm{R_\odot}$ (16:35 UT) in the COR1-A FOV.

In the future, this interpretation will be further tested based on the analysis of synthetic CME observations built starting from a full MHD 3D simulation, similar to what was recently done by Bemporad, Pagano, and Giordano (2018).

The values of the displacement of the CME during a polarisation sequence are summarised in Table 1.

Table 1 The displacement of the CME during a polarisation sequence. The first column shows the instrument taking the images, the second column displays the time at which a sequence of three polarised images was taken, the third column shows the speed of the CME in km s^{-1}, the fourth column shows the distance the CME travelled during the time interval the sequence was taken, which is displayed in column 5. The last column shows the displacement of the CME, in pixels, during the time interval that a sequence of three polarised images was taken.

Instrument	Time [hh:mm]	Speed [km s^{-1}]	Distance [km]	Duration [s]	Displacement [pixels]
COR1-A	16:35	600	10800	18	> 2
COR1-B	16:35	700	16800	24	> 2
COR2-A	17:08	1200	72000	60	> 3
COR2-B	17:08	1250	75000	60	> 3

4.3. CME Kinematics

We calculated the projected speeds of the CME's leading edge observed by COR1 and COR2 at its central position angle (PA). The PA is measured from the North Pole, counterclockwise. For LASCO-C2, where the CME was observed as a full halo, we take the values from the LASCO CME catalogue: cdaw.gsfc.nasa.gov/CME_list/. The speed was measured at the PA corresponding to the fastest-moving segment of the CME leading edge.

The values of the speeds as derived from different datasets are as follows:

- LASCO: speed of 885 km s^{-1} (linear fit), at a PA of 158°. From a second-order polynomial fit, the speed goes up to 1100 km s^{-1} at 5.5 R$_\odot$.
- COR1-A: speed from 200 km s^{-1} at around 2 R$_\odot$ (16:20 UT) to 1100 km s^{-1} at around 3.9 R$_\odot$ (16:55 UT), PA = 107°.
- COR1-B: speed from 500 km s^{-1} at around 2 R$_\odot$ (16:25 UT) to 900 km s^{-1} at around 3.2 R$_\odot$ (16:45 UT), PA = 254°.
- COR2-A: speed of 1000 km s^{-1}, at PA = 107° and height of 14 R$_\odot$ (18:39 UT) (decelerating from 1200 km s^{-1}).
- COR2-B: speed of 1250 km s^{-1}, at PA = 254° and height of 14 R$_\odot$ (18:24 UT) (slightly decelerating).

These values are shown also in Figure 8.

It is observed that the CME accelerates quite a lot in the regions of the corona below 4 R$_\odot$ and keeps approximately a constant speed above 4 R$_\odot$.

For a COR1 pixel size of 7.5″, i.e. 5245 km pixel^{-1} (COR1-A) and 5527 km pixel^{-1} (COR1-B), a CME moving at 1000 km s^{-1} will cross the single pixel in 5.24 seconds (COR1-A) and 5.53 seconds (COR1-B). This is larger than the nominal exposure time of one second. For a COR2 pixel size of 29.4″, i.e. 20,549 km pixel^{-1} (COR2-A) and 21,662 km pixel^{-1} (COR2-B), a CME moving at 1000 km s^{-1} will cross the single pixel in 20.55 seconds (COR2-A) and 21.66 seconds (COR2-B), which is again larger than the nominal exposure time of six seconds. Hence, plasma displacements during the exposure times can be neglected.

4.4. CME 3D Reconstruction

We applied three different reconstruction techniques in order to derive the 3D position of the CME, namely: triangulation model (Inhester, 2006), polarisation-ratio (PR) model (see,

Figure 8 Projected speeds versus height as measured in COR1-A at PA 107° (*black triangles*), COR1-B at PA 254° (*red squares*), COR2-A at 107° (*green triangles*), COR2-B at PA 254° (*orange squares*), and LASCO-C2 at 158° (*blue crosses*). The errors are derived by assuming an error in height of five pixels.
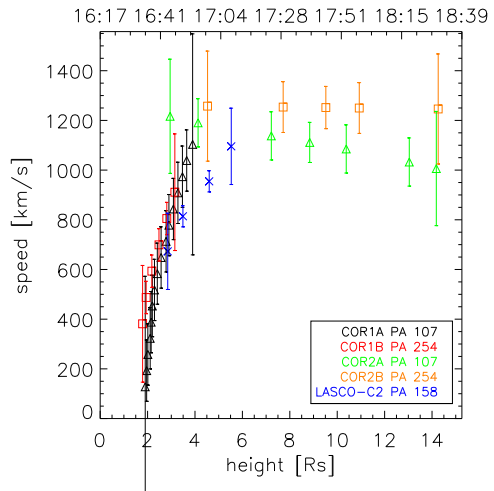
e.g., Moran and Davila, 2004; Dere, Wang, and Howard, 2005; Vourlidas and Howard, 2006; Floyd and Lamy, 2019), and a graduated cylindrical shell (GCS) model (see Thernisien, 2011).

The polarisation-ratio technique was applied on a small region at the central part of the CME leading edge and on the core of the CME, as seen in COR1-A at 16:35 UT. Triangulation was applied on the same regions. GCS was applied on the CME observed by COR1 at 16:35 and by COR2 at 17:08 UT. The results of GCS are displayed in Figure 9.

The results from different reconstruction techniques are summarised in Table 2 together with the location of STEREO-A, STEREO-B, and Earth on 12 July 2012 16:00 (also shown in Figure 10).

It is observed that the three methods, GCS, triangulation, and the polarised-ratio method, yield the same values for the position of the scattering material at distances around $2\,R_\odot$. At higher distances (around $6\,R_\odot$) the CME is slightly deflecting towards the Equator.

Given the position of the spacecraft and the direction of propagation of the CME, this was observed at i) the central meridian as seen from the Earth; ii) 30° behind the East limb as observed by STEREO-A and iii) 25° behind the West limb as observed by STEREO-B.

This is also visible in the STEREO/*Extreme Ultraviolet Imager* (EUVI) 195-A and -B data where dimmings appear as being located behind the limb (see, e.g., cdaw.gsfc.nasa. gov/stereo/daily_movies/2012/07/12/index.html).

5. Discussion

5.1. Discussion on the Degree of Polarisation

The degree of polarisation of the K-corona, depends on the distance from the solar surface and on the scattering angle to the observer. Besides the position in space of the structure (streamer, coronal mass ejection, etc.), the effective line-of-sight integration length is also important when deducing the degree of polarisation (Koutchmy, 1972).

We have found that the degree of polarisation is around 65% but it can go as high as 80% in some CME regions from COR1-A. Floyd and Lamy (2019) showed that for an electron
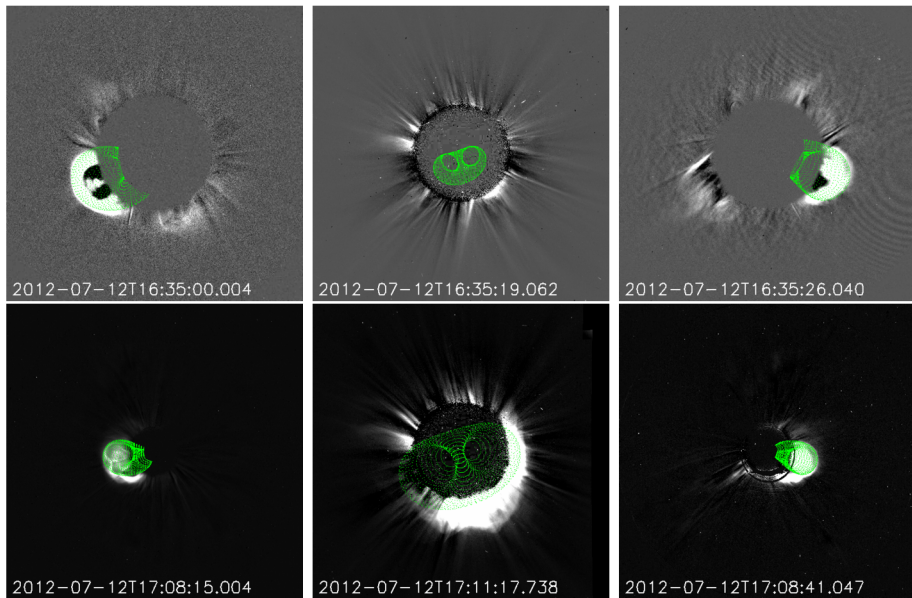
Figure 9 GCS reconstruction for the CME observed by STEREO/COR-A (*left panels*), LASCO-C2 (*middle panels*), and STEREO/COR-B (*right panels*) at around 16:35 UT (*upper panels*) and 17:08 (*lower panels*) on 12 July 2012.

Table 2 3D position of the CME as derived from different reconstruction techniques (in HEEQ coordinates; see Thompson, 2006). The last three entries show the positions of the spacecraft, also in HEEQ.

Time	lat/lon	Height	Feature	Technique	Instruments
16:00	S18W01	-	on-disk source	-	AIA
16:35	S18W05	2.48	LE	Triang.	COR1
16:35	S17E03	2.06	core	Triang.	COR1
16:35	S18W05	2.75	LE-A	PR	COR1
16:35	S16W05	2.15	core-A	PR	COR1
16:35	S18W00	2.5	LE	GCS	COR1 + C2
17:08	S07W00	5.7	LE	GCS	COR2 + C2
16:00	N04W00	-	-	-	Earth
16:00	N03W120	-	-	-	STEREO-A
16:00	S07E115	-	-	-	STEREO-B

in the POS at $2\,R_\odot$, the polarisation is about 0.8 and increases to nearly 1 at $3\,R_\odot$. These values decrease with increasing angle from the POS.

Similar or lower values of the degree of polarisation were observed for coronal streamers. Lamy et al. (2020) by studying polarised LASCO-C2 images showed that the brightest streamers culminate at a peak degree of polarisation of around 0.4 at $2.2\,R_\odot$, at the maximum of solar activity. Dürst (1982), by studying the solar eclipse of 16 February 1980, found that the degree of polarisation of the K-corona is strongly increasing with height in the inner corona, and it is almost constant for heights above $2\,R_\odot$. Several streamers located in or near the POS have maximum polarisation near 80%. Koutchmy, Picat, and Dantel (1977),

Figure 10 Position of the three spacecraft (STEREO-A (*red*), STEREO-B (*blue*), and SOHO - Earth perspective (*green*) on 12 July 2012, 16:00). The red arrow indicates the direction of propagation of the CME as derived from GCS reconstruction. The view is from above, in the Heliocentric Earth Ecliptic (HEE) coordinate system, with the *x*-axis towards the Earth and its *z*-axis towards the Ecliptic North Pole (Thompson, 2006).
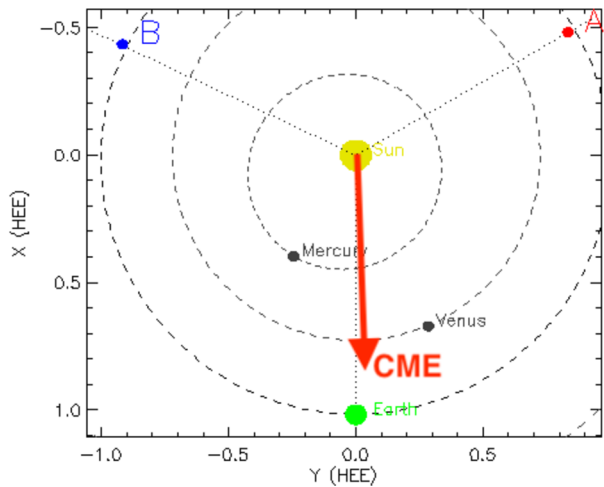
by studying the eclipse of 30 June 1973, found polarisations as high as 60% in regions associated with coronal streamers. In another solar-eclipse study, Vorobiev et al. (2020) found that the degree of polarisation of the F+K corona (including also the sky) peaks at around 47% in the equatorial features, at a distance of around $1.5 \, R_\odot$.

An unexpectedly large degree of polarisation (exceeding the maximum non-relativistic Thomson-scatter value) was observed by a number of authors (Koutchmy and Schatten, 1971; Pepin, 1970; Skomorovsky et al., 2012; Qu et al., 2013). This was attributed by Qu et al. (2013) to the contamination of the scattered white-light signal by coronal ion emission lines. As the majority of these studies were made during solar eclipses one extra source of contamination may come from the sky polarisation (see Koutchmy et al., 1999). Obviously this is not the case for space data.

5.2. Discussion on the Polarisation Angle

The anisotropy of the incident light causes the observed scattered radiation to exhibit a polarisation parallel to the visible solar limb (tangential to the solar limb).

In our case we observe deviations from the tangential greater than 10°, in regions associated with the CME brightness excess. Inhester et al. (2021) analysed COR1 observations of the quiescent corona and found a systematic constant deviation of the polarisation angle by $-1°$, which exceeded the calculated variance of the polarisation angle. As the most simple and most probable explanation, the authors proposed not-precise-enough knowledge of the orientation of the polarisers and thus an incorrect demodulation matrix. The offset of 2.5° in mechanical mounting of the polarisers in COR1 would provide a systematic deviation of order of 1°. Such an explanation is not applicable in our case, since the polarisation angle varies across the CME and takes larger values. We look for other possible explanation in the following sections.

5.3. Possible Interpretation of the Observed Deviation Angles: Relativistic Electrons?

It has been shown that deviation from the tangential may occur, and among possible physical reasons of such deviations we mention the Thomson scattering by the fast moving (relativis-

tic) electrons in the solar corona and the scattering by the supra-thermal electrons (Molodensky, 1973; Kishonkov and Molodenskii, 1975). These kinds of deviations have been reported only seldom in the literature (Pepin, 1970; Badalyan, 1988; Skomorovsky et al., 2012; Qu et al., 2013) and some results deduced from photographic films/plates are of limited precision and significance (Park et al., 2001; Kim and Popov, 2015), especially when radial neutral filters were not used. Other studies explicitly found no deviation from the tangential polarisation within the measurement error (Koutchmy et al., 1993; Filippov, Molodensky, and Koutchmy, 1994; Kim et al., 1996; Kulijanishvili and Kapanadze, 2005; Vorobiev et al., 2020).

In the case of a CME-driven shock wave the semi-relativistic electrons can be expected at the front or the flanks of the CME inducing radio emission (Type-II and Type-III radio bursts) (see, e.g., Claßen and Aurass, 2002; Magdalenić et al., 2014). The energies of impulsive electron events near the Sun could be in the range of $1-40$ keV (sometimes going down to 0.1 keV) (Reid and Ratcliffe, 2014). A small, e.g. order of 10%, population of high-energy electrons is sufficient to produce bursts. For a net rotation of the polarisation angle, the contribution of all electrons adds up incoherently. So if there are 10% beamed high-energy electrons their scatter with rotated polarisation adds to the unrotated Thomson background of the other 90%. This may strongly reduce the observed net rotation. If the electrons are not beamed but just isotropically heated, then each energetic electron in the tail of the distribution may rotate its scatter but if all contributions are added up this results not in a net observable rotation of the polarisation direction but just in a random broadening of the polarisation directions that probably is observed as a slightly reduced polarisation degree.

Small relativistic effects may be observed even for an electron energy of 0.03 keV with deviations relative to the non-relativistic limit of a few % for the degree of polarisation and two degrees away from the tangential direction for the polarisation angle (Inhester, 2015).

5.4. Possible Interpretation of the Observed Deviation Angles: Line Contamination?

The visible emission lines (Hα, Helium D3-line, Fe XIV, Fe X, etc.) are part of the signal of a coronagraph image together with the K-corona, F-corona, and the stray light.

As described in Section 3, COR1 observes in a white-light waveband 22.5 nm wide centred at the Hα line at 656 nm and COR2 observes in visible light with a passband from 650 to 750 nm. This implies that the CME signal observed by COR1 may be "contaminated" with Hα emission.

To investigate the potential contribution from Hα emission, we applied the polarisation-ratio technique on COR1-A data at 16:35. If the Hα contribution is significant we should observe low polarisation in the region of our CME (see, e.g., Poland and Munro, 1976; Mierla et al., 2011). Instead, from Figure 3 it is clear that a high degree of polarisation of order of 0.7 is observed in the CME region. Note also that the Hα emission is supposed to be observed in the core of the CME, but the deviation from the tangential was most visible in the leading edge.

Let us compare our reasoning with other events. As was pointed out by Floyd and Lamy (2019), the Helium D3 line at 587.7 nm, falls right at the centre of the LASCO-C2 orange bandpass and it was seen in the core of many three-part CMEs imaged by C2. The authors concluded that the prominence material embedded in LASCO CMEs is expected to have a maximum polarisation of the order of 17% and a direction somewhat deviating from the tangential. The same conclusion was derived from another study by Heinzel et al. (2020). In quiescent prominences, the polarisation of the He I D3 emission is low, typically 2% and its

direction deviates from the tangential by approximately $\pm 15°$ (Leroy, Ratier, and Bommier, 1977).

Dolei, Bemporad, and Spadaro (2014), by studying three blobs observed in COR1 images, demonstrated that the Hα contribution to the total white-light intensity observed at the location of the blobs is between 95 and 98%. They also showed that the Hα polarised component is of the order of a few percent of the Hα total emission from the blobs.

Mierla et al. (2011) demonstrated that the major part of a CME core emission (more than 85%) is Hα radiation, and only a small fraction is Thomson-scattered light. This results in the reduction of the CME polarisation signal. The CME was associated with a filament eruption, and it was observed by the COR1 instrument.

The same was deduced from the eclipse of 2019 with the CATE experiment (D. Elmore, private communication, 2021). They observed a prominence at the NNE limb with polarisation close to zero over the polarised coronal background.

For this study, EUV images at 304 and 195 Å taken by EUVI and the *Solar Dynamics Observatory/Atmospheric Imaging Assembly* (AIA) were inspected and no filament/prominence was found. Nevertheless, the CME had a three-part structure with a bright leading edge, followed by a dark cavity and a bright core, meaning it was a flux-rope-like ejecta. Such CMEs without any associated filaments are often reported in the literature, e.g. Howard et al. (2017) and Vourlidas et al. (2013). From the 3D reconstruction described above we saw that the two methods, triangulation and the polarisation-ratio, yield the same values for the position of the scattering material.

Thus, we can conclude that there is no Hα emission associated with our CME, i.e. the signal of the CME is due entirely to the Thomson-scattered light.

5.5. Other Effects That Can Modify the Polarisation Angle and the Degree of Polarisation

Other phenomena that can create low polarisation in coronagraph images are F-corona emission (e.g. Morgan and Habbal, 2007) and Thomson scattering from enhanced plasma density far away from the POS (e.g. Billings, 1966). The F-corona contribution is ruled out because it forms a diffuse background and does not vary rapidly in time. The subtraction of the image taken 45 minutes before our image at 16:35 should have removed any F-corona contribution.

As shown above, the CME appears at different locations in each polarised image resulting in an error in the measured polarisation. This effect may be taken care of by binning the images. Thernisien, Vourlidas, and Howard (2011) showed that substantial binning of the LASCO-C2 images would be required to suppress the effect, for instance by a factor of about 36 (from the original format of 1024×1024 pixels) for a CME travelling at 500 km s^{-1}.

We performed a similar test with the COR1-A image at 16:35 UT. By binning the image to a size of 64×64 (i.e. 16 times less than the original image) we noted that the deviation angle from the tangential is around $0 \pm 3°$, while in the binned 128×128 images one can still see small deviations (around $7°$), especially in the front part of the CME. In these regions, the original image can have a deviation as high as $15°$ or more (see Figure 3). The binned images of 32×32 were too noisy to conclude anything.

The degree of polarisation for the binned images behaves in a similar way to the deviation angle images, i.e. the high values (above 0.65) decrease or disappear with the size of the image.

5.6. Discussion on Different Effects Influencing the Polarisation Analysis

In a recent study by Floyd and Lamy (2019), the main limitations the authors encountered when deriving the polarisation parameters of 15 CMEs observed by LASCO-C2 were: i) the

contamination of the LASCO-C2 passband filter with the He I D3 line at 587.7 nm. ii) the duration of ten minutes of a LASCO-C2 polarisation sequence resulting in the blurring of the polarisation in the case of the fast CMEs. The front of fast CMEs appeared at different locations in each polarised image resulting in an error in the measured polarisation. iii) using a pre-event image resulted in artifacts affecting the *pB*-images of the LASCO-C2 CMEs because traces of underlying coronal structures are interfering with the CME signal.

In another study, Lamy et al. (2020), using the newest calibrated LASCO-C2 polarised images, analysed the polarised K-corona over the two complete Solar Cycles 23 and 24, and they compare it with a variety of eclipse data taken during the two solar cycles. The agreement with the eclipse data is in general good except for slight discrepancies affecting the innermost part of the C2 field of view.

To do this analysis, the authors needed to introduce further corrections to the polarised data: i) the correction for the global transmission of the 0° polariser; ii) global correction function applied to polarised images; iii) exposure-time equalisation of the three polarised images. They showed that errors on the relative global transmission between polarisers and on the individual exposure times of the triplet forming a polarisation sequence have similar effects, which were corrected by an optimisation procedure based on imposing a tangential direction to the solar limb of polarisation and minimal dispersion around this direction. They concluded that the capability of LASCO-C2 to perform accurate polarimetric measurements is affected by several adverse conditions, prominently the very basic polarisation analyser system (three Polaroid foils), the optical design with two folding mirrors, and the fluctuations in exposure times.

A similar study was performed by Lamy et al. (2021), this time with the newest calibrated LASCO-C3 polarised data. They only used two polarisers in this case, because of the degradation of the 0° polariser.

In the case of internally occulted coronagraphs (like COR1) multiple reflections in the instrument from the direct photospheric light are difficult to avoid. When using an externally occulted instrument simulating a total eclipse (LASCO-C2, COR2, etc.), the photospheric light does not reach the instrument, but several new problems appear, as described by Lamy et al. (2020). Some significant improvement was made in the case of the COR1 and COR2 coronagraphs by using a rotating single polariser instead of comparing images taken using different polarisers, as was done with LASCO-C2. However, in the case of COR1 and COR2, although polarisation images are taken through the same optics, the rotation of the polariser introduces some wobble between the images due to the fact that the front and rear surfaces of the polariser are not exactly parallel. This effect is smaller than a pixel, but the slight misregistration between the three images can produce some spurious polarisation signals at sharp transitions in brightness (see, e.g., the analysis of the Comet Lovejoy by Thompson (2015)). This is definitely an issue when analysing comet data, but is not generally a problem for the solar corona, where the variations in brightness tend to be more gradual. In our case the effect is negligible compared to other sources of uncertainty.

To summarise, the causes affecting the polarimetric measurements may be related to i) the instrument design: e.g. the optical design with two folding mirrors, as in the case of LASCO-C2; the basic polarisation analyser system (three Polaroid foils as in LASCO-C2, and one polariser that rotates as in COR). ii) the instrumental operation mode: e.g. the fluctuations in exposure times; the time difference in taking a polarisation sequence (ten minutes for LASCO-C2, a few seconds for COR1 and COR2). iii) the correct extraction of the K-corona signal from other signals (different background subtractions are involved). iv) contamination of the bandpass with emission lines (He I D3 for LASCO-C2 and Hα for COR1).

From the effects specified above, the one affecting most of our measurements is related to the time span in taking a polarisation sequence. The other effects are minimised by our data pre-processing (with the secchi_prep routine), by background subtraction (to keep only the CME K-corona signal – see the discussion in Appendix B) and by the type of the observation (CME without any prominence associated, i.e. no emission-line contamination).

5.7. Improving the Polarisation Analysis

The question arises of how we can improve polarisation measurements of CMEs. Of course, one aspect is low scattered light, but this is not the key aspect since scattered light is subtracted by the pre-event image. Key areas of improvement are the accuracy, hence the technique (three polaroids being the worst) and the speed of the measurements (to "freeze" the motion of the CMEs).

The *Solar Orbiter visible light and ultraviolet coronal imager* (Metis: Antonucci et al., 2020) has the technical capability of obtaining polarisation measurements of quality superior to those of LASCO-C2 and COR1 thanks to its electro-optical device, which does not require any mechanical motion. The resulting much faster mode of operation will contribute to the reduction of the time delays between the individual images required to obtain the deviation-angle image.

One step forward to improve the derivation of the polarisation parameters was proposed by Vorobiev et al. (2020). The authors used a new polarimetric imaging camera and method: a set of four linear micro-polarisers at 0, 45, 90, and 135° put over each "sub-matrix" made of "super pixels" of 2×2 assembled on the CCD chip. They could detect polarisation signals as small as 0.3% and found no strong deviations in the angle of linear polarisation from the tangential direction.

Koutchmy et al. (2019a,b) also performed such analyses by using a rotating linear Polaroid placed in front of the entrance lens of F300 mm at F/5.6 and a Canon D60 color CMOS camera of 24 Mpx. Twelve images were recorded at positions consecutively shifted by 15°, with a precision better than one degree and a cadence of four seconds using the same exposure time of 1/8 second. No deviation from the tangential direction was found (at the 1° level of precision) after subtracting the sky background, as measured over the image of the Moon.

Among the next space missions with new polarisation technical developments is BITSE (*Balloon-borne Investigation of Temperature and Speed of Electrons*) in the corona (see Gong, Gopalswamy, and Newmark, 2019). BITSE's detector will be able to directly collect polarised light at four different wavelengths: 385.0, 398.7, 410.0, and 423.3 nm. It will measure the coronal average electron temperature using the Grotrian method.

PUNCH (*Polarimeter to UNify the Corona and Heliosphere*) will also have polarisation capability. It comprises four matched cameras all operating as a "virtual instrument" to image Thomson-scattered light, from the vantage of four separate spacecraft in Sun-synchronous LEO. PUNCH is the first coronal and solar-wind imager designed specifically to produce three-dimensional images from a single vantage point (DeForest et al., 2019).

The future externally occulted coronagraph ASPIICS (*Association of Spacecraft for Polarimetric and Imaging Investigation of the Corona of the Sun*), onboard PROBA-3 (*Project for On-Board Autonomy*), will be the first space-borne instrument to image the polarised corona at distances as low as $1.1 \, R_\odot$, with low stray light (Lamy et al., 2010; Renotte et al., 2015; Galano et al., 2018). The coronagraph will be equipped with a filter wheel with six positions to choose between three spectral filters and three linear polarisers. ASPIICS will not suffer from radial vignetting due to its remote external occulter and it will preserve its

image quality throughout its FOV. Nevertheless, due to the usage of a filter wheel there will be limitations because of the non-simultaneity in taking the set of three polarised images.

6. Conclusions

In this work we have used SECCHI/COR1 and COR2 polarised white-light data to study a large and fast CME on 12 July 2012. We used the degree of polarisation to calculate the position of the CME in 3D. We compared it with the position derived from triangulation and forward-modelling techniques, and we found very good agreement among them. From the study of the CME kinematics we derived projected speeds up to around 1000 km s^{-1}. The CME studied here showed deviation of the polarisation angle from the tangential in the range of $10 - 15°$ (or more). Our analysis showed that this is mostly due to the fact that the sequence of three polarised images from which the polarised parameters are derived is not taken simultaneously, but at a difference of few seconds in time. In this interval of time, the CME moves by at least two pixels in the FOV of the instruments, and this displacement results in uncertainties in the polarisation parameters (degree of polarisation, polarisation angle, etc.).

We conclude that the observational effect of the propagation of the CME front through the image combined with non-simultaneous polarisation observations is the most likely reason for the deviation of the polarisation angle from the tangential direction. To our knowledge this effect has not been considered before.

This study is important also for analysing future data from instruments with polarisation capabilities.

Appendix A: Background Subtraction

In order to keep signal only from the K-corona, one can employ different procedures on raw white-light coronagraph images:

i) subtraction of the monthly minimum background from a raw white-light coronagraph image. The monthly minimum background is created by taking the minimum in each pixel over a four-week period of daily median images. It removes the static K-corona, the F-corona, and the stray light from the images, assuming that the F-corona and the stray light do not change much during a one-month period. Overall, this procedure works well but it can remove also parts of the stable K-corona (and parts of F-corona and stray light may still be present in the image).

ii) subtraction of a previous image from a raw white-light coronagraph image. This is mostly used for studying K-corona dynamic features like CMEs. One can subtract a pre-event image (the so-called base-difference image technique) or the preceding image (the so-called running-difference image technique) in order to keep only the signal from the dynamic feature we are interested in. Nevertheless, static features and the E-corona signal may still be present in the final image. The main assumption here is that the stray light and F-corona do not vary over few minutes/hours.

iii) subtraction of a hourly minimum background from a raw white-light coronagraph image. This is also suitable for dynamic features. The background is built by taking the minimum value in each pixel of all images over a time range of eight hours, centred at the launch time of the CME. As a result, we should obtain the brightness of the CME alone. Nevertheless, static features and the E-corona signal may still be present in the final image.

Within the field of view of COR1, the dominant signal is the K-corona (when compared with the F-corona). However, because of the COR1 design (no external occulter) the instrumental stray light is very high.

For COR2 (and LASCO) the F-corona is the dominant signal in the images. The instrumental stray light in COR2 is very low (especially when compared to COR1).

As a consequence, the COR1 and COR2 monthly minimum background images are fundamentally different. The COR1 monthly minimum background image (subtracted as part of secchi_prep) is used to remove instrumental stray light. The COR2 monthly minimum background images (not removed within secchi_prep) are used to remove the F-corona signal.

In our study we used different background images for COR1 data. The COR1 monthly minimum background subtracted images should leave us only with the K-corona signal. If any F-corona signal is left it should be unpolarised in the COR1 FOV and it should not influence the polarisation angle. Nevertheless, it is not guaranteed that the full stray light is removed by this background. On the other hand, when using the base-difference images, due to the short time between the two images, any contribution from stray light and F-corona should be removed. However, also part of the stable K-corona is removed, leaving us in theory only with the CME K-corona signal. The hourly minimum background subtraction, obtained over a time range of eight hours centred at the launch time of the CME should remove all the unwanted signal and leave us only with the brightness of the CME alone; similar with base-difference images.

Appendix B: The Influence of Different Background Subtractions

Here, we compare the COR1 base-difference images with the monthly minimum background-subtracted images and with the hourly minimum background subtracted images (see Figure 11), in order to see if different backgrounds influence our results.

The hourly minimum background-subtracted images are very similar to base-difference images, while the monthly minimum background subtracted images show a poorer quality of the data. We suspect this is because the stray light may be still present in these images.

As described in Appendix A not one of the above-mentioned backgrounds is perfect. Nevertheless, all of them point to the same result: deviations higher than 10° of the polarisation angle from the tangential, in all pixels where a significant CME excess brightness is observed (see Figure 11).
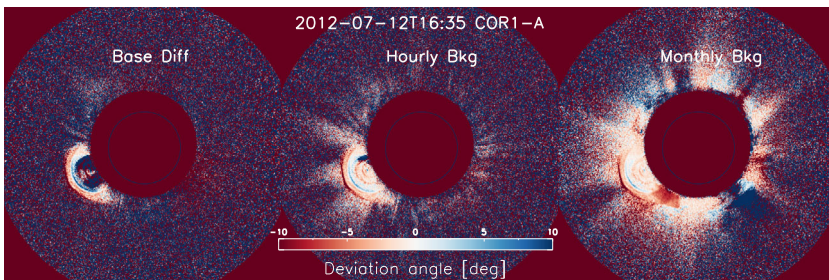
Figure 11 Deviation angle for COR1-A image at 16:35 with the base image subtracted (*left panel*), hourly minimum background subtracted (*middle panel*) and monthly minimum background subtracted (*right panel*).

Data Availability All the data used in this study (SECCHI-COR1, -COR2, LASCO-C2, and AIA) are publicly available and can be downloaded from the corresponding instrument webpages.

Declarations

Disclosure of Potential Conflicts of Interest The authors declare that they have no conflicts of interest.

References

Antonucci, E., Romoli, M., Andretta, V., Fineschi, S., Heinzel, P., Moses, J.D., Naletto, G., Nicolini, G., Spadaro, D., Teriaca, L., Berlicki, A., Capobianco, G., Crescenzio, G., Da Deppo, V., Focardi, M., Frassetto, F., Heerlein, K., Landini, F., Magli, E., Marco Malvezzi, A., Massone, G., Melich, R., Nicolosi, P., Noci, G., Pancrazzi, M., Pelizzo, M.G., Poletto, L., Sasso, C., Schühle, U., Solanki, S.K., Strachan, L., Susino, R., Tondello, G., Uslenghi, M., Woch, J., Abbo, L., Bemporad, A., Casti, M., Dolei, S., Grimani, C., Messerotti, M., Ricci, M., Straus, T., Telloni, D., Zuppella, P., Auchère, F., Bruno, R., Ciaravella, A., Corso, A.J., Alvarez Copano, M., Aznar Cuadrado, R., D'Amicis, R., Enge, R., Gravina, A., Jejčič, S., Lamy, P., Lanzafame, A., Meierdierks, T., Papagiannaki, I., Peter, H., Fernandez Rico, G., Giday Sertsu, M., Staub, J., Tsinganos, K., Velli, M., Ventura, R., Verroi, E., Vial, J.-C., Vives, S., Volpicelli, A., Werner, S., Zerr, A., Negri, B., Castronuovo, M., Gabrielli, A., Bertacin, R., Carpentiero, R., Natalucci, S., Marliani, F., Cesa, M., Laget, P., Morea, D., Pieraccini, S., Radaelli, P., Sandri, P., Sarra, P., Cesare, S., Del Forno, F., Massa, E., Montabone, M., Mottini, S., Quattropani, D., Schillaci, T., Boccardo, R., Brando, R., Pandi, A., Baietto, C., Bertone, R., Alvarez-Herrero, A., García Parejo, P., Cebollero, M., Amoruso, M., Centonze, V.: 2020, Metis: the Solar Orbiter visible light and ultraviolet coronal imager. *Astron. Astrophys.* **642**, A10. DOI. ADS.

Badalyan, O.G.: 1988, Evidence for coronal expansion based on electron component data. *Astron. Zh.* **65**, 403. ADS.

Baumbach, S.: 1938, Die Polarisation der Sonnenkorona. *Astron. Nachr.* **267**, 273. DOI. ADS.

Bemporad, A., Pagano, P., Giordano, S.: 2018, Measuring the electron temperatures of coronal mass ejections with future space-based multi-channel coronagraphs: a numerical test. *Astron. Astrophys.* **619**, A25. DOI. ADS.

Billings, D.E.: 1966, *A Guide to the Solar Corona*. Academic Press, New York. ADS.

Brueckner, G.E., Howard, R.A., Koomen, M.J., Korendyke, C.M., Michels, D.J., Moses, J.D., Socker, D.G., Dere, K.P., Lamy, P.L., Llebaria, A., Bout, M.V., Schwenn, R., Simnett, G.M., Bedford, D.K., Eyles, C.J.: 1995, The Large Angle Spectroscopic Coronagraph (LASCO). *Solar Phys.* **162**, 357. DOI. ADS.

Claßen, H.T., Aurass, H.: 2002, On the association between type II radio bursts and CMEs. *Astron. Astrophys.* **384**, 1098. DOI. ADS.

Decraemer, B., Zhukov, A.N., Van Doorsselaere, T.: 2019, Three-dimensional density structure of a solar coronal streamer observed by SOHO/LASCO and STEREO/COR2 in quadrature. *Astrophys. J.* **883**, 152. DOI. ADS.

DeForest, C.E., Gibson, S.E., Beasley, M., Colaninno, R.C., Killough, R., Kosmann, W., Laurent, G.T., McMullin, D.R.: 2019, Polarimeter to UNify the corona and heliosphere (PUNCH): imaging the corona and solar wind as a single system. In: *AGU Fall Meeting Abstracts* **2019**, SH43B. ADS.

Dere, K.P., Wang, D., Howard, R.: 2005, Three-dimensional structure of coronal mass ejections from LASCO polarization measurements. *Astrophys. J. Lett.* **620**, L119. DOI. ADS.

Dolei, S., Bemporad, A., Spadaro, D.: 2014, Measurements with STEREO/COR1 data of drag forces acting on small-scale blobs falling in the intermediate corona. *Astron. Astrophys.* **562**, A74. DOI. ADS.

Dürst, J.: 1982, Two colour photometry and polarimetry of the solar corona of 16 February 1980. *Astron. Astrophys.* **112**, 241. ADS.

Feng, L., Wang, Y., Shen, F., Shen, C., Inhester, B., Lu, L., Gan, W.: 2015, Why does the apparent mass of a coronal mass ejection increase? *Astrophys. J.* **812**, 70. DOI. ADS.

Filippov, B.P., Molodensky, M.M., Koutchmy, S.: 1994, On the optical polarization of the white-light coronal structures. In: Rusin, V., Heinzel, P., Vial, J.-C. (eds.) *IAU Colloq. 144: Solar Coronal Structures*, Veda, Bratislava, 601. ADS.

Floyd, O., Lamy, P.: 2019, Polarimetric reconstruction of coronal mass ejections from LASCO-C2 observations. *Solar Phys.* **294**, 168. DOI. ADS.

Galano, D., Bemporad, A., Buckley, S., Cernica, I., Dániel, V., Denis, F., de Vos, L., Fineschi, S., Galy, C., Graczyk, R., Horodyska, P., Jacob, J., Jansen, R., Kranitis, N., Kurowski, M., Ladno, M., Ledent, P., Loreggia, D., Melich, R., Mollet, D., Mosdorf, M., Paschalis, A., Peresty, R., Purica, M., Radzik, B., Rataj, M., Rougeot, R., Salvador, L., Thizy, C., Versluys, J., Walczak, T., Zarzycka, A., Zender, J., Zhukov, A.: 2018, Development of ASPIICS: a coronagraph based on Proba-3 formation flying mission. In: Lystrup, M., MacEwen, H.A., Fazio, G.G., Batalha, N., Siegler, N., Tong, E.C. (eds.) *Space Telescopes and Instrumentation 2018: Optical, Infrared, and Millimeter Wave*, Soc. Photo-Opt. Instrument. Eng. (SPIE) **CS-10698**, 106982Y. DOI. ADS.

Gong, Q., Gopalswamy, N., Newmark, J.: 2019, Innovative compact coronagraph approach for Balloon-borne Investigation of Temperature and Speed of Electrons in the corona (BITSE). In: *Astronomical Optics: Design, Manufacture, and Test of Space and Ground Systems II*, Soc. Photo-Opt. Instrument. Eng. (SPIE) **CS-11116**, 111160F. DOI. ADS.

Heinzel, P., Štěpán, J., Bemporad, A., Fineschi, S., Jejčič, S., Labrosse, N., Susino, R.: 2020, On the possibility of detecting helium D3 line polarization with metis. *Astrophys. J.* **900**, 8. DOI. ADS.

Howard, R.A., Moses, J.D., Vourlidas, A., Newmark, J.S., Socker, D.G., Plunkett, S.P., Korendyke, C.M., Cook, J.W., Hurley, A., Davila, J.M., Thompson, W.T., St Cyr, O.C., Mentzell, E., Mehalick, K., Lemen, J.R., Wuelser, J.P., Duncan, D.W., Tarbell, T.D., Wolfson, C.J., Moore, A., Harrison, R.A., Waltham, N.R., Lang, J., Davis, C.J., Eyles, C.J., Mapson-Menard, H., Simnett, G.M., Halain, J.P., Defise, J.M., Mazy, E., Rochus, P., Mercier, R., Ravet, M.F., Delmotte, F., Auchere, F., Delaboudiniere, J.P., Bothmer, V., Deutsch, W., Wang, D., Rich, N., Cooper, S., Stephens, V., Maahs, G., Baugh, R., McMullin, D., Carter, T.: 2008, Sun Earth Connection Coronal and Heliospheric Investigation (SECCHI). *Space Sci. Rev.* **136**, 67. DOI. ADS.

Howard, T.A., DeForest, C.E., Schneck, U.G., Alden, C.R.: 2017, Challenging some contemporary views of coronal mass ejections. II. The case for absent filaments. *Astrophys. J.* **834**, 86. DOI. ADS.

Illing, R.M.E., Hundhausen, A.J.: 1986, Disruption of a coronal streamer by an eruptive prominence and coronal mass ejection. *J. Geophys. Res.* **91**, 10951. DOI. ADS.

Inhester, B.: 2006, Stereoscopy basics for the STEREO mission. arXiv. ADS.

Inhester, B.: 2015, Thomson Scattering in the Solar Corona. arXiv. ADS.

Inhester, B., Mierla, M., Shestov, S., Zhukov, A.N.: 2021, Error estimation of linear polarization data from coronagraphs - application to STEREO-a/SECCHI-COR1 observations. *Solar Phys.* **296**, 72. DOI. ADS.

Kaiser, M.L., Kucera, T.A., Davila, J.M., St. Cyr, O.C., Guhathakurta, M., Christian, E.: 2008, The STEREO mission: an introduction. *Space Sci. Rev.* **136**, 5. DOI. ADS.

Kim, I.S., Popov, V.V.: 2015, Manifestations of electric currents observed in the K-corona. *Geomagn. Aeron.* **55**, 1131. DOI. ADS.

Kim, I.S., Bougaenko, O.I., Belenko, I.A., Koutchmi, S., Matsuura, O.T., Picazzio, E.: 1996, The coronograph-polarimeter: an algorithm for creation of solar corona polarization images. *Radiophys. Quantum Electron.* **39**, 869. DOI. ADS.

Kishonkov, A.K., Molodenskii, M.M.: 1975, Precise determination of the orientation of the plane of polarization in the solar corona. *Solar Phys.* **42**, 341. DOI. ADS.

Koutchmy, S.: 1972, Étude hydrodynamique du grand jet coronalne observé à I'éclipse du 7 Mars 1970. *Solar Phys.* **24**, 373. DOI. ADS.

Koutchmy, S., Picat, J.P., Dantel, M.: 1977, Etude polarimétrique de la couronne solaire observe a l'èclipse totale du 30 juin 1973 à l'aide d'un filtre neutre radial. *Astron. Astrophys.* **59**, 349. ADS.

Koutchmy, S., Schatten, K.H.: 1971, Observations and discussions concerning 'high' polarization features in the solar corona. *Solar Phys.* **17**, 117. DOI. ADS.

Koutchmy, S., Molodenskii, M.M., Nikol'skii, G.M., Filippov, B.P.: 1993, Measuring the polarization of the solar corona. *Astron. Rep.* **37**, 286. ADS.

Koutchmy, S., Matsuura, O., Molodensky, M.M., Picazzio, E., Starkova, L.I.: 1999, The plane of polarization of the solar corona during eclipse observations. *Astron. Rep.* **43**, 198. ADS.

Koutchmy, S., Filippov, B., Lecleire, J.M., Lefaudeux, N., Mouette, J., Sèvre, F., Tavabi, E., Viladrich, C., Abdi, S.: 2019, Eclipse 2017: new results on the dynamical inner-corona. In: Di Matteo, P., Creevey, O., Crida, A., Kordopatis, G., Malzac, J., Marquette, J.-B., N'Diaye, M., Venot, O. (eds.) *SF2A-2019: Proc. Annual Meeting of the French Society of Astronomy and Astrophysics*. ADS.

Koutchmy, S., Baudin, F., Abdi, Sh., Golub, L., Sèvre, F.: 2019, New deep coronal spectra from the 2017 total solar eclipse. *Astron. Astrophys.* **632**, A86. DOI. ADS.

Kulijanishvili, V.I., Kapanadze, N.G.: 2005, Polarization and physical properties of the August 11, 1999 white-light corona. *Solar Phys.* **229**, 45. DOI. ADS.

Lamy, P., Damé, L., Vivès, S., Zhukov, A.: 2010, ASPIICS: a giant coronagraph for the ESA/PROBA-3 Formation Flying Mission. In: Oschmann, J.M. Jr., Clampin, M.C., MacEwen, H.A. (eds.) *Space Telescopes and Instrumentation 2010: Optical, Infrared, and Millimeter Wave*, Soc. Photo-Opt. Instrument. Eng. *(SPIE)* **CS-7731**, 773118. DOI. ADS.

Lamy, P., Barlyaeva, T., Llebaria, A., Floyd, O.: 2014, Comparing the solar minima of cycles 22/23 and 23/24: the view from LASCO white light coronal images. *J. Geophys. Res.* **119**, 47. DOI. ADS.

Lamy, P., Llebaria, A., Boclet, B., Gilardy, H., Burtin, M., Floyd, O.: 2020, Coronal photopolarimetry with the LASCO-C2 coronagraph over 24 years [1996 - 2019]. *Solar Phys.* **295**, 89. DOI. ADS.

Lamy, P., Gilardy, H., Llebaria, A., Quémerais, E., Ernandez, F.: 2021, LASCO-C3 observations of the K- and F-coronae over 24 years (1996 - 2019): photopolarimetry and electron density distribution. *Solar Phys.* **296**, 76. DOI. ADS.

Magdalenić, J., Marqué, C., Krupar, V., Mierla, M., Zhukov, A.N., Rodriguez, L., Maksimović, M., Cecconi, B.: 2014, Tracking the CME-driven shock wave on 2012 March 5 and radio triangulation of associated radio emission. *Astrophys. J.* **791**, 115. DOI. ADS.

Mierla, M., Inhester, B., Marqué, C., Rodriguez, L., Gissot, S., Zhukov, A.N., Berghmans, D., Davila, J.: 2009, On 3D reconstruction of coronal mass ejections: I. Method description and application to SECCHI-COR data. *Solar Phys.* **259**, 123. DOI. ADS.

Mierla, M., Chifu, I., Inhester, B., Rodriguez, L., Zhukov, A.: 2011, Low polarised emission from the core of coronal mass ejections. *Astron. Astrophys.* **530**, L1. DOI. ADS.

Minnaert, M.: 1930, On the continuous spectrum of the corona and its polarisation. *Z. Astrophys.* **1**, 209. With 3 figures. (Received July 30, 1930). ADS.

Molodensky, M.M.: 1973, On an anomalous polarization of the corona. *Solar Phys.* **28**, 465. DOI. ADS.

Moran, T.G., Davila, J.M.: 2004, Three-dimensional polarimetric imaging of coronal mass ejections. *Science* **305**, 66. DOI. ADS.

Morgan, H., Habbal, S.R.: 2007, The long-term stability of the visible F corona at heights of 3-6 $R_\odot$. *Astron. Astrophys.* **471**, L47. DOI. ADS.

Park, Y.-D., Kim, I.S., Bugaenko, O.I., Divlekeev, M.I., Popov, V.V., Dermenjiev, V.N.: 2001, The plane of polarization of the solar coronal emission on August 11, 1999. *Astron. Rep.* **45**, 729. DOI. ADS.

Pepin, T.J.: 1970, Observations of the brightness and polarization of the outer corona during the 1966 November 12 total eclipse of the sun. *Astrophys. J.* **159**, 1067. DOI. ADS.

Poland, A.I., Munro, R.H.: 1976, Interpretation of broad-band polarimetry of solar coronal transients: importance of the Halpha emission. *Astrophys. J.* **209**, 927. DOI. ADS.

Qu, Z.Q., Deng, L.H., Dun, G.T., Chang, L., Zhang, X.Y., Cheng, X.M., Allington-Smith, J., Murray, G., Qu, Z.N., Xue, Z.K., Ma, L.: 2013, On the combination of imaging-polarimetry with spectropolarimetry of upper solar atmospheres during solar eclipses. *Astrophys. J.* **774**, 71. DOI. ADS.

Quémerais, E., Lamy, P.: 2002, Two-dimensional electron density in the solar corona from inversion of white light images - application to SOHO/LASCO-C2 observations. *Astron. Astrophys.* **393**, 295. DOI. ADS.

Reid, H.A.S., Ratcliffe, H.: 2014, A review of solar type III radio bursts. *Res. Astron. Astrophys.* **14**, 773. DOI. ADS.

Renotte, E., Alia, A., Bemporad, A., Bernier, J., Bramanti, C., Buckley, S., Capobianco, G., Cernica, I., Dániel, V., Darakchiev, R., Darmetko, M., Debaize, A., Denis, F., Desselle, R., de Vos, L., Dinescu, A., Fineschi, S., Fleury-Frenette, K., Focardi, M., Fumel, A., Galano, D., Galy, C., Gillis, J.-M., Górski, T., Graas, E., Graczyk, R., Grochowski, K., Halain, J.-P.A., Hermans, A., Howard, R., Jackson, C., Janssen, E., Kasprzyk, H., Kosiec, J., Koutchmy, S., Kovačičinová, J., Kranitis, N., Kurowski, M., Ładno, M., Lamy, P., Landini, F., Lapáček, R., Lédl, V., Liebecq, S., Loreggia, D., McGarvey, B., Massone, G., Melich, R., Mestreau-Garreau, A., Mollet, D., Mosdorf, L., Mosdorf, Ł., Mroczkowski, M., Muller, R., Nicolini, G., Nicula, B., O'Neill, K., Orleański, P., Palau, M.-C., Pancrazzi, M., Paschalis, A., Patočka, K., Peresty, R., Popescu, I., Psota, P., Rataj, M., Rautakoski, J., Romoli, M., Rybecký, R., Salvador, L., Servaye, J.-S., Solomon, C., Stockman, Y., Swat, A., Thizy, C., Thomé, M., Tsinganos, K., Van der Meulen, J., Van Vooren, N., Vit, T., Walczak, T., Zarzycka, A., Zender, J., Zhukov, A.: 2015, Design status of ASPIICS, an externally occulted coronagraph for PROBA-3. In: Fineschi, S., Fennelly, J. (eds.) *Solar Physics and Space Weather Instrumentation VI*, Soc. Photo-Opt. Instrument. Eng. *(SPIE)* **CS-9604**, 96040A. DOI. ADS.

Shklovskii, I.S.: 1965, *Physics of the Solar Corona*. Pergamon, Oxford. ADS.

Shopov, Y.Y., Stoykova, D.A., Stoitchkova, K., Tsankov, L.T., Tanev, A., Burin, K., Belchev, S., Rusanov, V., Ivanov, D., Stoev, A., Muglova, P., Iliev, I.: 2008, Structure of the solar dust corona and its interaction with the other coronal components. *J. Atmos. Solar-Terr. Phys.* **70**, 356. DOI. ADS.

Skomorovsky, V.I., Trifonov, V.D., Mashnich, G.P., Zagaynova, Y.S., Fainshtein, V.G., Kushtal, G.I., Chuprakov, S.A.: 2012, White-light observations and polarimetric analysis of the solar corona during the eclipse of 1 August 2008. *Solar Phys.* **277**, 267. DOI. ADS.

Thernisien, A.: 2011, Implementation of the graduated cylindrical shell model for the three-dimensional reconstruction of coronal mass ejections. *Astrophys. J. Suppl.* **194**, 33. DOI. ADS.

Thernisien, A., Vourlidas, A., Howard, R.A.: 2011, CME reconstruction: pre-STEREO and STEREO era. *J. Atmos. Solar-Terr. Phys.* **73**, 1156. DOI. ADS.

Thompson, W.T.: 2006, Coordinate systems for solar image data. *Astron. Astrophys.* **449**, 791. DOI. ADS.

Thompson, W.T.: 2015, Linear polarization measurements of comet C/2011 W3 (lovejoy) from STEREO. *Icarus* **261**, 122. DOI. ADS.

Thompson, W.T., Reginald, N.L.: 2008, The radiometric and pointing calibration of SECCHI COR1 on STEREO. *Solar Phys.* **250**, 443. DOI. ADS.

van de Hulst, H.C.: 1950, The electron density of the solar corona. *Bull. Astron. Inst. Neth.* **11**, 135. ADS.

Vorobiev, D., Ninkov, Z., Bernard, L., Brock, N.: 2020, Imaging polarimetry of the 2017 solar eclipse with the RIT polarization imaging camera. *Publ. Astron. Soc. Pac.* **132**, 024202. DOI. ADS.

Vourlidas, A., Howard, R.A.: 2006, The proper treatment of coronal mass ejection brightness: a new methodology and implications for observations. *Astrophys. J.* **642**, 1216. DOI. ADS.

Vourlidas, A., Wu, S.T., Wang, A.H., Subramanian, P., Howard, R.A.: 2003, Direct detection of a coronal mass ejection-associated shock in large angle and spectrometric coronagraph experiment white-light images. *Astrophys. J.* **598**, 1392. DOI. ADS.

Vourlidas, A., Lynch, B.J., Howard, R.A., Li, Y.: 2013, How many CMEs have flux ropes? Deciphering the signatures of shocks, flux ropes, and prominences in coronagraph observations of CMEs. *Solar Phys.* **284**, 179. DOI. ADS.

Authors and Affiliations

Marilena Mierla[1,2] · **Bernd Inhester[3]** · **Andrei N. Zhukov[1,4]** ·
Sergei V. Shestov[1] · **Alessandro Bemporad[5]** · **Philippe Lamy[6]** · **Serge Koutchmy[7]**

✉ M. Mierla
marilena.mierla@oma.be

B. Inhester
inhester@mps.mpg.de

A.N. Zhukov
andrei.zhukov@oma.be

S.V. Shestov
sergei.shestov@oma.be

A. Bemporad
alessandro.bemporad@inaf.it

P. Lamy
philippe.lamy@latmos.ipsl.fr

S. Koutchmy
koutchmy@iap.fr

[1]   Solar-Terrestrial Centre of Excellence - SIDC, Royal Observatory of Belgium, Avenue Circulaire 3, Brussels 1180, Belgium

[2]   Institute of Geodynamics of the Romanian Academy, Bucharest, Romania

[3]   Max-Planck-Institute for Solar System Research, Göettingen, Germany

[4]   Skobeltsyn Institute of Nuclear Physics, Moscow State University, 119992 Moscow, Russia

[5]   INAF-Turin Astrophysical Observatory, Turin, Italy

[6]   Laboratoire Atmospheres, Milieux et Observations Spatiales, CNRS & UVSQ, Guyancourt, France

[7]   Institut d'Astrophysique de Paris, CNRS and Sorbonne University, Paris, France